J. Ziebs, J. Meersmann,* H.-J. Kühn,* and S. Ledworuski**

Experimental Techniques for Testing Materials Under Multiaxial Loading

REFERENCE Ziebs, J., Meersmann, J., Kühn, H. J., and Ledworuski, S., **Experimental techniques for testing materials under multiaxial loading**, *Multiaxial Fatigue and Design*, ESIS 21 (Edited by A. Pineau, G. Cailletaud, and T. C. Lindley) 1996, Mechanical Engineering Publications, London, pp. 173–193.

ABSTRACT Multiaxial testing techniques are reviewed. Specimen geometry and stress–strain gradients are seen to have a significant influence on the results of multiaxial loading. The thin-walled tube is used as smooth specimen for multiaxial fatigue. Due to the large number of testing machines available for multiaxial loading the experimental equipment and therefore methods have become very varied among different investigators and laboratories. Establishing common frameworks within this field is considered. Increased understanding of the detailed micromechanisms for cyclic deformation and fatigue failure represents an important challenging direction.

1 Introduction

Most structural members and machine components are subjected to multiaxial stress–strain conditions due to geometrical configuration, discontinuities and/or temperature fluctuations, Fig. 1. In such cases principal stresses may be nonproportional and the principal directions can often change throughout the component's load cycle of life. Finite endurance limits, calculated using the predicted service life, are therefore used in the design of components and structures subject to conditions of multiaxial loading. It is clear that, in order to improve the accuracy of fatigue criteria, reliable experimental methods must be selected.

This paper briefly reviews existing multiaxial fatigue loading systems and outlines the requirements of the experimental methods needed to obtain reliable fatigue results under various load configurations and for different specimens. Comprehensive descriptions of these methods are also given in Refs (**1–5**). The importance of using loading methods which ensure that all possible $\varepsilon_2/\varepsilon_1$ ratios (where ε_1, ε_2 are principal strains), with reference to local multiaxial stress–strain states and stress–strain gradients, is discussed. Often factors considered include

*Federal Institute for Materials Research and Testing, Unter den Eichen 87, D-12205, Berlin, Germany.

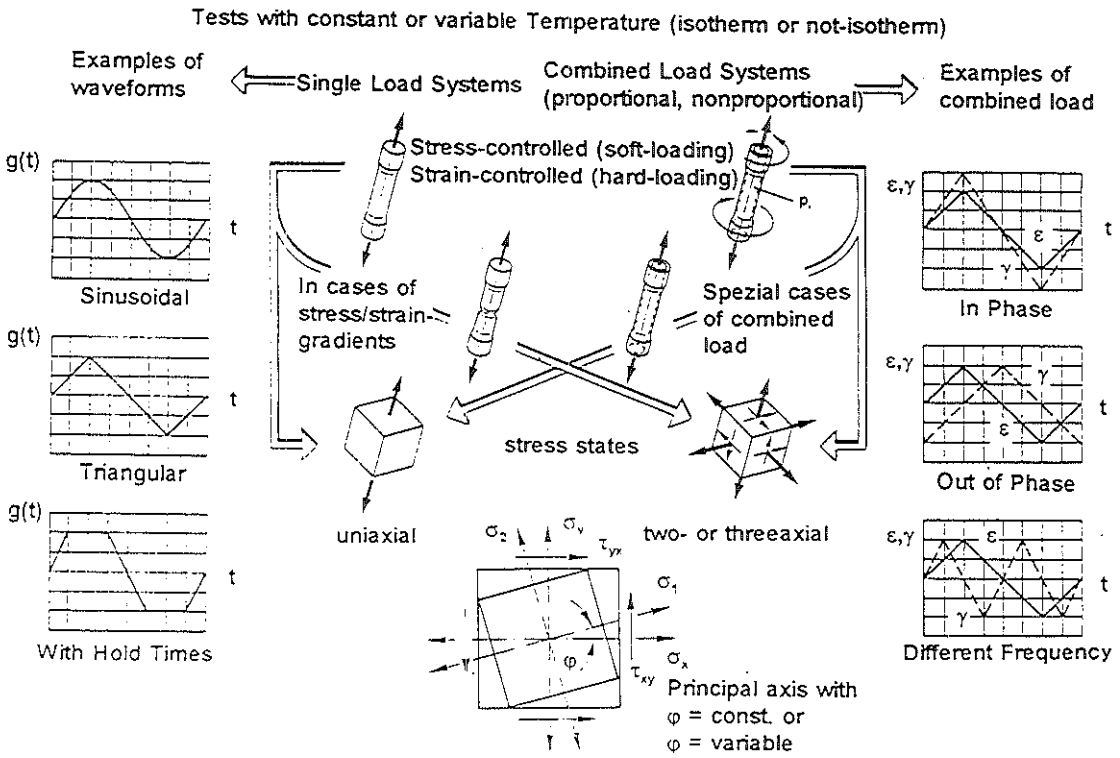

Fig 1 Definition of multiaxial loading.

changes in principal axis positions, specimen design, grip design, strain measuring methods, alignment of loading, thermomechanical testing and controlling and monitoring and recording of loading parameters. It is noted that the effects of test variations cannot be adequately assessed due to lack of specified experimental procedures. It is therefore obvious that some standardization is required to allow comparisons of results from various sources to be made.

The development of servo-hydraulic testing machines and associated closed-loop control systems has opened up new possibilities for tests under complex stress–strain conditions. However, the large variety of systems available inevitably leads to a large variety of experimental methods among the different investigators and laboratories. Establishing common frameworks for performing multiaxial tests and reporting results would encourage more widespread utilization of resulting data.

2 General Testing Methodology

Tests are diverse as they attempt to simulate the actual stress patterns found in particular components or to simulate a homongenous (strictly speaking, any inhomogeneity present is in most cases negligible), uniquely determinable stress–strain state. A homogenous test would, for example, subject a cylindrical thin-walled tube to simultaneous force-controlled tension, torsion and internal pressure. The process at any point of the specimen is controlled by axial stress σ_x, tangential stress σ_y and shear stress τ_{xy}. These values are determined irrespective of the system of coordinates adopted. Such a test can be applied, if the stress distribution in the body is statically determinable or if the strain distribution is geometrically determinable. It should be noted, however, that in general with an arbitrarily shaped body and arbitrary external loadings, it is very difficult to calculate the stress–strain components at a given point of the body.

Due to the large number of test methods and configurations, a comprehensive assessment of the advantages and disadvantages of all methods is not attempted in this article. Possible multiaxial tests, however, include:

- Thin-walled cylindrical specimens under combinations of tension, torsion, internal and external pressure, open- and closed-end specimens.
- Cruciform loading of plate specimens and of three-dimensional configurations.
- Notched specimens.
- Plate-type specimens such as bulging plate, wide cantilever plate (beam) and rhombic plate under bending.
- Pressurized thick-walled tubes.

3 Correlation of Multiaxial Stress–Strain Behaviour

The above-mentioned multiaxial loadings may be controlled by various independent external forces, F_i, by displacements and by parameter character-

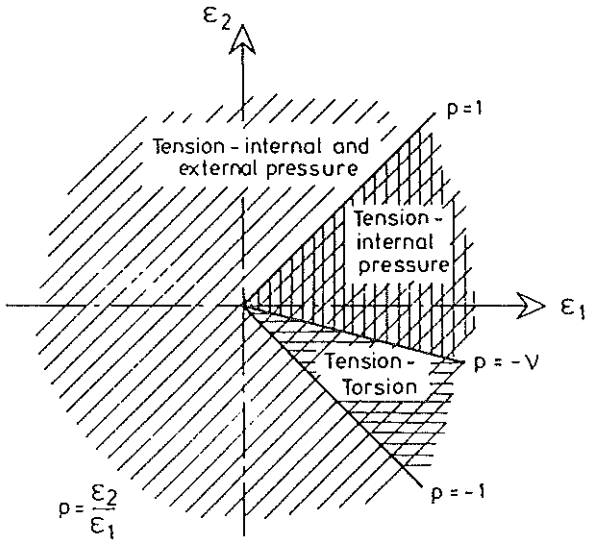

Fig 2 The range of strain ratio covered in multiaxial loading.

izing the temperature distribution. The essential feature of multiaxial loadings is the independence of the individual loading parameters. Assuming symmetry of the stress tensor, in general, there are six independent stress components and six strain components.

Fatigue failures occur when the strain field is below the elastic limit. The crack is initiated at a localized point of cyclic plasticity which can be so small that the component as a whole is observed to respond in a purely elastic manner. Under these conditions the study of fatigue damage is usually based on the intensity of stress or strain (von Mises theory).

In low-cycle fatigue a significant and measurable plastic component of strain exists and various attempts have been made to relate this existence to fatigue failure. Modified yield theories, the maximum shear strain (with or without a combination of the normal strain on this shear plane) and strain energy have been used to predict multiaxial high-strain fatigue (**16–18**).

To correlate experimental data on multiaxial fatigue, the effective stress $\bar{\sigma}$ and effective plastic strain $\bar{\varepsilon}$ are defined in terms of principal components as follows (von Mises)

$$\bar{\sigma} = \frac{1}{\sqrt{2}} [(\sigma_1 - \sigma_2)^2 + (\sigma_2 - \sigma_3)^2 + (\sigma_3 - \sigma_1)^2]^{1/2} \tag{1}$$

$$\bar{\varepsilon} = \frac{1}{(1+\nu)\sqrt{2}} [(\varepsilon_1 - \varepsilon_2)^2 + (\varepsilon_2 - \varepsilon_3)^2 + (\varepsilon_3 - \varepsilon_1)^2]^{1/2} \tag{2}$$

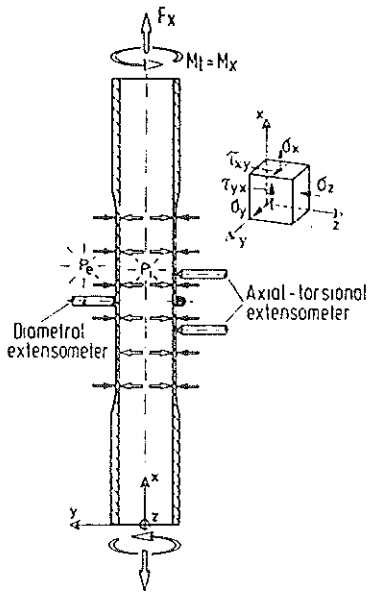

Fig 3 An axisymmetric homogeneous thin-walled tube is statically determinate.

In the second formula two extreme conditions may be distinguished: $\nu = 0.3$ (elastic case) and $\nu = 0.5$ (fully plastic case). In states of multiaxial imposed stress, Poisson's ratio influences the resultant strains in all the directions of imposed stresses. The effective Poisson's ratio in fatigue significantly differs from $\nu = 0.5$ due to the influence of multiaxial stress and strain fields. For steels which show slight cyclical hardening over a long period, tested at room temperature, a value of $\nu_{fat} = 0.3$ is a good approximation (9).

An explicit relation can be found between the maximum shear strain, γ_{max}, and the normal strain on the maximum shear plane, ε_n, when the principal strains are ordered, i.e. $\varepsilon_1 > \varepsilon_2 > \varepsilon_3$, then $\gamma_{max} = \varepsilon_1 - \varepsilon_3$ and $\varepsilon_n = (\varepsilon_1 + \varepsilon_2)/2$.

4 Multiaxial Loadings

Mulitiaxial fatigue data at room or high temperature is greatly influenced by test procedure and conditions. Numerous methods have been suggested for multiaxial loading, however only a limited number have been successfully performed. One important requirement of multiaxial loading tests is the ability to achieve a full range of biaxial strain ratios $\rho = \varepsilon_2/\varepsilon_1$ ($\varepsilon_1 > \varepsilon_2$ principal strains) throughout the test. This is done by using a selection of test systems and specimen shapes, Fig. 2. The most damaging conditions occur when the strain ratio $\varepsilon_2/\varepsilon_1$ is positive.

4.1 *Thin-walled tubes under combined loadings*

The state of stress in thin-walled tubes under tension and torsion plus internal and external pressure is both transversely and longitudinally homogeneous, Fig. 3. Thus, the corresponding axial stress $\sigma_x = \sigma_x(t)$, circumferential stress $\sigma_y = \sigma_y(t)$, radial stress $\sigma_z = \sigma_z(t)$ and shear stress $\tau_{xy} = \tau_{xy}(t)$ are determined from the measured axial force, torque and internal and external pressure as follows (t indicates that these quantities vary with time)

$$\sigma_x = 4F/\pi(d_e^2 - d_i^2) \tag{3}$$

$$\sigma_y = (p_i - p_e)(d_e + d_i)/2(d_e - d_i) \tag{4}$$

$$\sigma_z \approx -(p_i + p_2)/2 \tag{5}$$

$$\tau_{xy} = \frac{M}{2\pi r^2 h} \tag{6}$$

where d_i and d_e = internal and external diameters; h = thickness of wall; r = mid-radius of wall; F = fluctuating axial force after correction for internal and external pressure effects; p_i and p_e = internal and external pressures.

At any point in the tube, four independent strains $\varepsilon_x(t)$, $\varepsilon_y(t)$, $\varepsilon_z(t)$ and $\gamma_{xy}(t)$ and interrelated strains in the directions of all imposed normal stresses due to Poisson's ratio occur.

The advantage of this specimen loading is that the three load systems can in principle be applied independently, as well as simultaneously, in-phase or out-of-phase. However, the principal stresses vary in a complicated manner, which can be related to a function of time and space. In the previous discussion it was assumed that displacements were small, i.e., we considered only infinitesimal strains. When finite strains are investigated, then certain problems arise. For example, the circumferential stress increases not only because of the decreasing cross-sectional area, but also because of the increasing tube diameter. Therefore, due to experimental difficulties particularly in measuring and controlling strains, experiments have so far been limited in the main to simultaneous application of two load systems (tension–torsion or tension–internal pressure) only.

Tension–torsion experiments

Simultaneous tension and torsion in components occurs frequently. The principal directions and the ratio of principal stresses in these components alter constantly. In such combined loadings tests the ratio $\rho = \varepsilon_2/\varepsilon_1$ of the in-plane principal strain varies within a narrow range $-\nu$ to -1, (see Fig. 2). Principal strain values and directions are determined from simple analysis and consideration of Mohr's circle in strain space, Fig. 4. Conditions of plane stress may be assumed, resulting in ε_x. ε_y and ε_z are the Poisson's contractions equal to $-\nu\varepsilon_x$ in the y- and z-direction. Shear strains γ_{xy} are also applied. In experimental

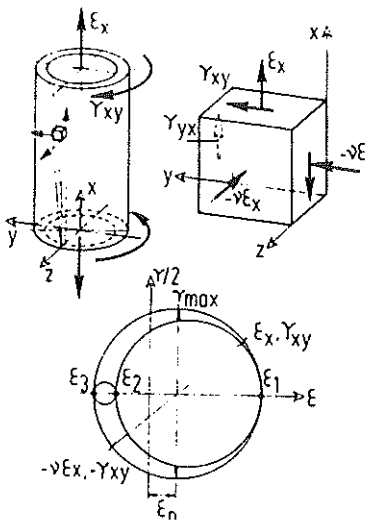

Fig 4 Strain analysis for thin-walled tube under tension–torsion.

programmes strains (stresses) are to be controlled to the desired values by computer-controlled double-channel closed-loop servo-hydraulic testing systems using an axial–torsional extensometer. The resulting data is the stress (strain) history experienced by a given strain-(stress), to simulate hard (soft) loading. During torsional loading there is a slight stress gradient from the inside surface to the outside surface of the wall.

In strain-controlled tension–torsion biaxial cyclic loading axial and torsional strains are given as (sinusoidal wave form)

$$\varepsilon = \varepsilon_{ax} \sin(\omega t), \quad \gamma_{xy} = \gamma_{xy} \sin(\omega t - \phi) \tag{7}$$

where ε_x = axial strain; γ_{xy} = torsional strain; ε_{ax} = axial strain amplitude; γ_{ay} = torsional strain amplitude; ω = angular frequency; ϕ = phase angle. The elimination of the common parameter 'ωt' gives

$$(\varepsilon_x/\varepsilon_{ax})^2 + (\gamma_{xy}/\gamma_{axy})^2 - 2(\varepsilon_x/\varepsilon_{ax})(\gamma_{xy}/\gamma_{axy}) \cos\phi = \sin^2\phi \tag{8}$$

This equation represents different shapes in the ε–γ space depending on the magnitude of the phase angle ϕ.

In biaxial testing two strains (ε, γ) are usually measured. However, in order to calculate principal strains and other values it is necessary to know the full strain tensor. This is achieved by assuming an effective Poisson's ratio. The assumptions made about the Poisson's ratio can significantly affect the calculated values of various parameters used to correlate cyclic multiaxial loading data. In the case of tension–torsion loading there is almost no

T K	Strain Path	N at $\dot{\bar{\varepsilon}}$= $10^{-3}s^{-1}$	Angle of main crack	N at $\dot{\bar{\varepsilon}}$= $10^{-6}s^{-1}$	Angle of main crack
298	⊖	6, 1		30,26	
	⊖	5778		>245	
	⊘	1328			
	○	3, 4		9	
		5		12	
923	⊖	21		18	
	⊖	238		502	
	⊘	67		42	
	○	2, 4		36	
1023	⊖	23		>170	
	⊖	520		121	
	⊘	63		38	
	○	13		8	
1123	⊖	45, 35		10	
	⊖	90, 80	45° 45°	57	
	⊘	24,70,75		36	
	○	>20,11	55° 45° 45°	10	
1223	⊖	50		8	
	⊖	70	60° 45°	18	45°
	⊘	45	45°	10	
	○	8		14	

Fig 5 Orientation of the main fracture paths and cycles to fracture of proportional and nonproportional straining paths, IN 738 LC.

circumferential plastic strain and therefore volume is conserved by a large strain in a direction through the tube wall. Therefore it seemed appropriate to measure this strain in the direction through the tube wall.

It can be also difficult to accurately measure the displacements (strains) as axial strain is accumulated in reversed torsion and torsional strain in reversed tension. Axial, torsional and combined axial–torsional cyclic loadings were applied to IN 738 LC as an example of a tension–torsion test. Figure 5 shows

how the orientation of the main fracture paths of the thin-walled specimens increase from 90° to 135° as the ratio $\Delta\gamma_{xy}/\Delta\varepsilon_x$ increases from zero (uniaxial) to infinity (torsional) (angles are measured in the clockwise direction from the specimen axis).

Tension–internal and/or external pressures

In the simplest combined case, that is tension with internal pressure, there are biaxial stress states with fixed principal directions. However, in this loading method the strain ratio $\rho = \varepsilon_2/\varepsilon_1$ is limited to the range $-\nu \leqslant \rho \leqslant 1$ and cannot provide a fully reversed strain cycle, Fig. 2.

With both internal and external pressure fully reversed cycling can be achieved and therefore tests of any strain path in the ε_1, ε_2 space can be carried out, Fig. 3 (**2, 5, 10**). Two principal strains ε_x (axial strain) and ε_y (circumferential strain) are controlled and the third one ε_z (radial strain) is to be calculated. Radial strain is difficult to measure but represents a significant proportion of the strain, being of the same order of magnitude as the other two strain components. Usually, it is assumed that the radial stress σ_z is zero. This however is not the case as a steep stress gradient exists across the thin-walled tube from the inside to the outside. The ratio of the maximum radial stress to the circumferential stress varies with the thickness of the tube. For the ratio r/h (r = radius of tube, h = thickness) $\gg 1$ the stress σ_z is negligible compared to the stresses σ_x and σ_y.

Torsion and internal pressure

Thin-walled tubular specimens may also be subjected to torsion and internal pressure. In this instance, the change of the principal directions is related to the ratio of the principal stresses. Loading produces a circumferential normal stress σ_y and a longitudinal shear stress τ_{xy} in the tube wall. If no loading compensation is made for the axial tension induced by the internal pressure, an axial normal stress $\sigma_x = \sigma_y/2$ is also induced. The test method gives $\varepsilon_2/\varepsilon_1$ ratios in the range of $-\nu \leqslant \rho \leqslant -1$, but cannot provide fully reversed cycling.

4.2 *Cruciform specimens*

A wide range of strain ratios $\varepsilon_2/\varepsilon_1$ was obtained in the central region of a cruciform specimen, Fig. 6, by altering the levels and phasing of the loads under static or cylic loading conditions (**11, 12**). The shape of the specimen has been calculated by finite-element methods. The specimen design is made up of a series of limbs extending from each edge of a thin central square test section. In the cruciform specimen strain distribution is not as uniform in the cruciform specimen as in the thin-walled tube and strain measurement is more difficult due to variation in thickness. This type of specimen is generally used for studying crack growth under biaxial stress (load) conditions.

A three-dimensional cruciform specimen with six arms was also designed. Severe stress raisers are present in this type of specimen making it impossible

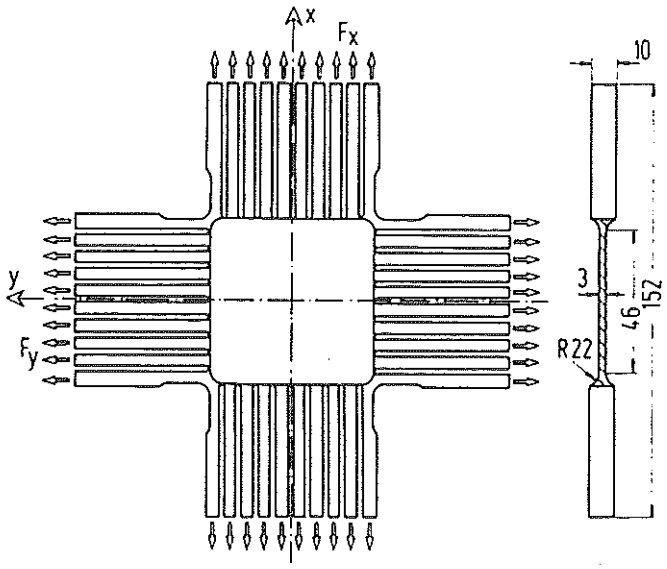

Fig 6 Cruciform specimen.

to gain a homogeneous strain or stress distribution. This inhomogeneous triaxial stress or strain state has a major effect on the fatigue properties.

4.3 *Notched circular specimens*

Combined loading cases can be achieved using a 'notched' specimen, Fig. 7. The specimen geometry and the loading configuration result not only in triaxial stresses and strains in the notch, but also in three-dimensional stress–strain gradients. The stress and strain ranges at the notch root can be determined using the finite-element method, the image processing method, the modified Neuber rule and others. However, the change in notch geometry during a test modifies the original stress state. A further disadvantage of this technique is that the initial stress distribution at the root of the notch can relax to an 'intermediate' stress state, which is then further changed by redistributions. Nominal axial or nominal axial–shear stress controlled tests may be carried out (13). A new laser-shadow-method can be used to measure the displacement and alteration of the notch root radius using a gauge length of 0.1 mm. The obtained displacements can then be used to determine a test control value, Fig. 8.

4.4 *Plate specimens*

This group includes three simplified types of tests that can be conducted on flat plate specimens:

(1) cantilever bending

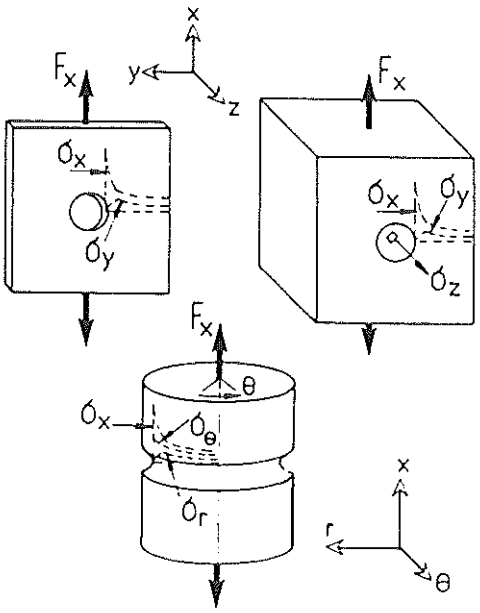

Fig 7 Elastically calculated stresses in several types of notched specimens.

(2) square or rhombic plate
(3) circular or elliptical (oval) plate.

The variable of the cantilever beam gives biaxial stress states $\nu \geqslant \lambda \geqslant 0$ where $\lambda = \sigma_y/\sigma_x$ The state of stress produced by antielastic bending of 'rhombic' plates depends on the ratio of major to minor axes $0 > \lambda \geqslant 1$, Fig. 9.

Four other types of circular and elliptical specimens are used as shown in Fig. 10. The stress state covers $1 > \lambda > \nu$. All tests can run under completely reversed deflection control. However, this class of tests, although easily applicable, cannot cover a wide range of test conditions. A stress analysis of the loading system is also required to gain an understanding of the results. Further complications arise, due to the influence of the stress–strain gradients and to the indeterminable influence of the specimen changing geometry.

4.5 *Thick-walled tubes under internal pressure*

In pressurized thick-walled tubes subjected to internal pressure (closed end) a triaxial stress state exists (σ_x, σ_y σ_z = axial, circumferential, radial stress). Circumferential and equivalent stresses are maximized at the inner wall.

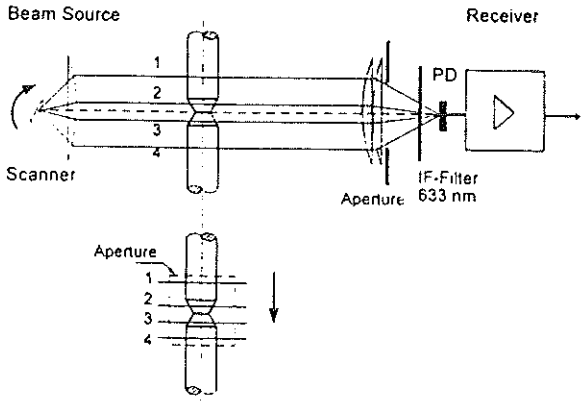

Fig 8 Laser-shadow method.

5 Test Machine and Control System

Multiaxial tension–torsion internal pressure servo-hydraulic machines are available commercially including extensometry to measure axial and torsional displacements together with a temperature-controlled induction heating unit. Figure 11 shows the testing unit schematically. There are several closed-loops for axial, torsional and internal force and temperature. For good loop stability and performance it is important to adjust the loop gain controls. The machine has a fixed response time which prevents instantaneous load changes or

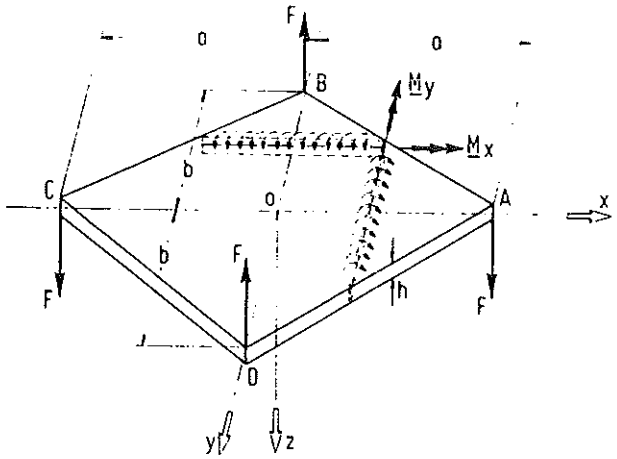

Fig 9 Test specimen configuration used in bending studies (14).

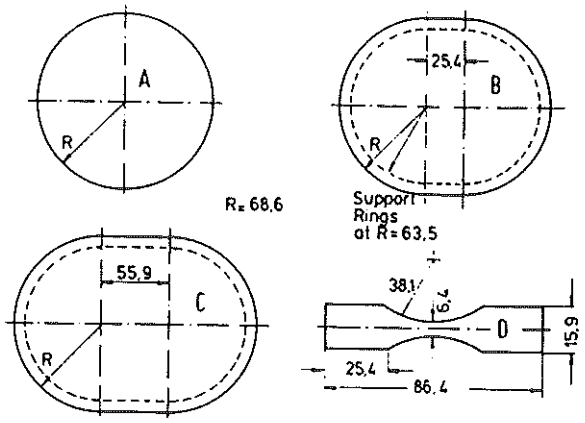

Fig 10 Test method and specimen used in (15).

displacement rates. This limitation caused more difficulties for variable temperature testing than had previously been anticipated. This slow response generally results from a combination of the inherent machine characteristics and the control system. Different test conditions, such as different test temperatures, will change the rate-dependent character of the test specimen and consequently the nonlinear character of the system will be altered. The use of an extensometer as a feedback transducer to remove machine compliance does not eliminate this problem although it does eliminate the uncertainty associated with both test machine compliance and nonlinearities.

Static or cylic internal pressure is achieved using Helium gas generated by intensifier equipment and introduced through the upper fixing collet. The intensifier generates pressures of up to 210 bar.

The internal pressure can be combined with end loading of the tube. The system energy in a pressurized tube depends on the volume of pressurizing gas. This is generally kept as low as possible by using a stone filler bar inside the tube. However, it must always be taken into account that when the tube is axially loaded the diameter of the tube will be reduced.

Water-cooled collet grips are used for holding the specimen. The collets provide adequate gripping capability when the specimens are inserted to an adequate depth.

Alignment in the elastic and plastic region is to be checked using a specimen with strain gauges, Fig. 12. The effect of superimposing nonaxiality of loading is to increase the measured overall strain. Induction heating offers the advantage of a fast thermal response and is therefore used for fatigue and thermomechanical fatigue testing. Careful coil design provides uniform temperature distribution in the specimen gauge section at the required temperature levels and also provides sufficient access to connect instruments to specimens and to allow the

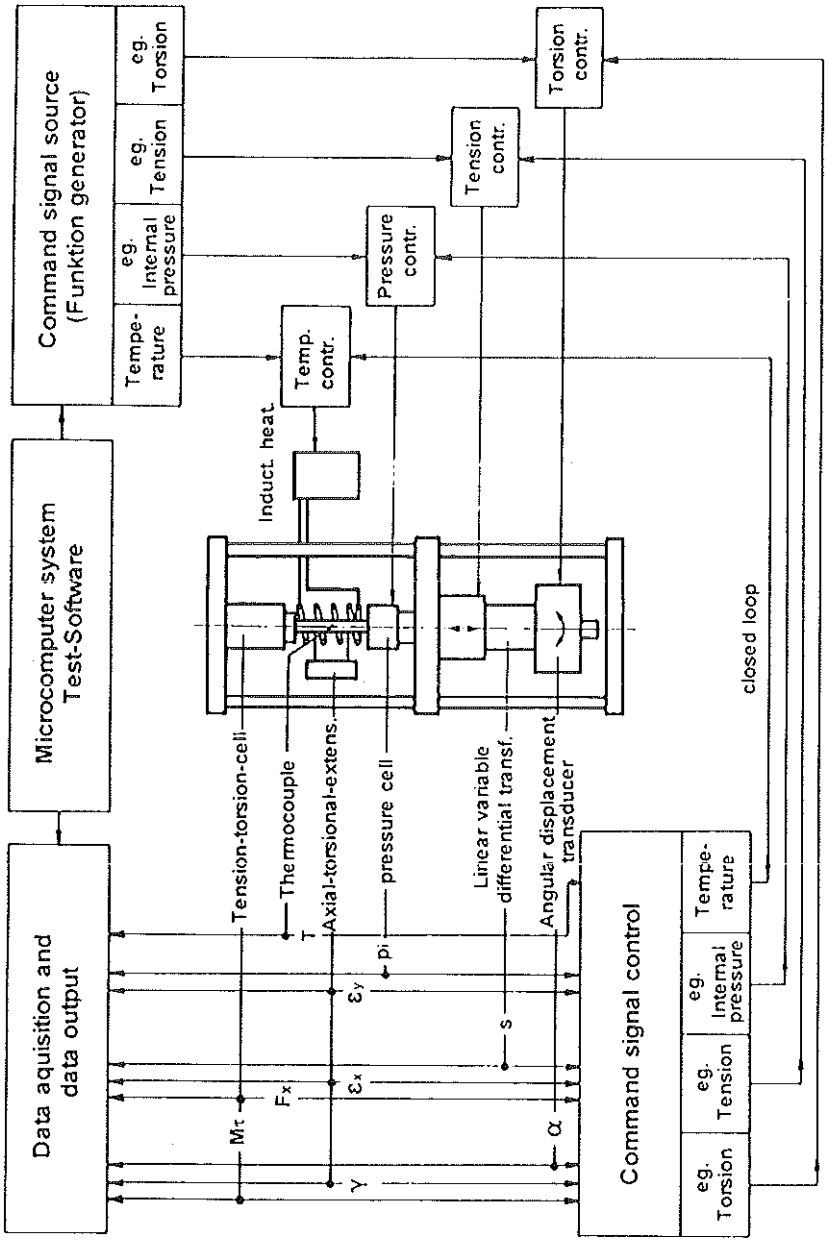

Fig 11 Tension–torsion internal pressure testing machine together with a induction heating.

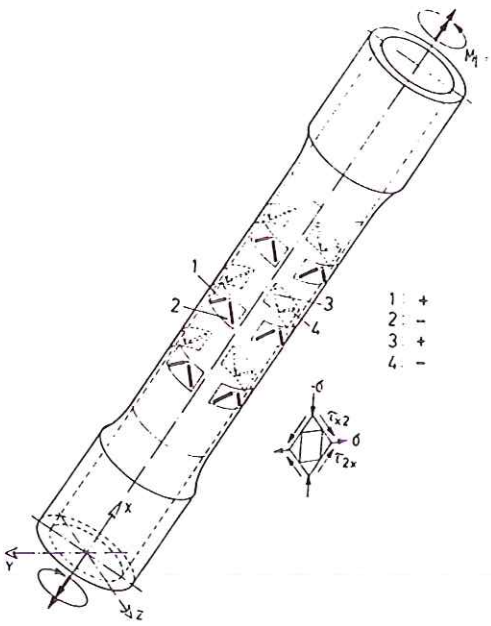

Fig 12 The determination of bending on tubular specimens under torsion.

specimen surface to be replicated. The potential problem of local crack tip heating, due to the crack concentrating the induction field, is relevant in multi-axial fatigue because of the multi-directionality of the cracking. Another modification could be to include two water cooling collars which clamp to the specimen between the heater and the grips to prevent heat transfer to the collet grips.

6 Specimen Design

Two basic types of specimen geometry are most frequently used for multi-axial fatigue test: the cruciform specimen and the thin-walled cylinder. Due to difficulties mentioned above with cruciform specimens thin-walled tubes were chosen as the specimen shape in most investigations. This type of geometry gives the following advantages.

(1) easy measurements of the different components of stress and strain;
(2) at high temperatures thermal gradients across the wall thickness are minimal;
(3) for thermomechanical tests cooling rates are higher;
(4) the relatively large, uniformly strained gauge length which permits the installation of strain transducers.

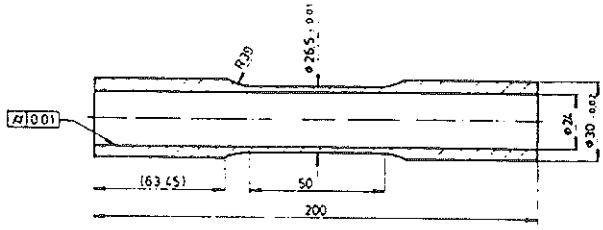

Fig 13 Thin-walled tubular specimen.

The specimen design, shown in Fig. 13, is a compromise of the two conflicting requirements of uniform strain field and resistance to buckling. For a tubular specimen the geometrical factors affecting the onset of instability are wall thickness, axial length and diameter. The strain monitoring during cycling should be restricted to a small gauge length in the central portion of the specimen. With different radii at each end of the gauge length we can observe axial–strain waveform profiles with the maximum peaks nearest to the fillet. The introduction of an internal pressure increases the buckling as can clearly be seen in Fig. 14, which shows the profile of a steel tube tested under tension, torsion and internal pressure. The application of internal pressures induces longitudinal as well as circumferential bending moments (**15**). Specimen end shoulders could develop a barrel shape on high strain loading so that complex bending strains are superimposed on the loading system.

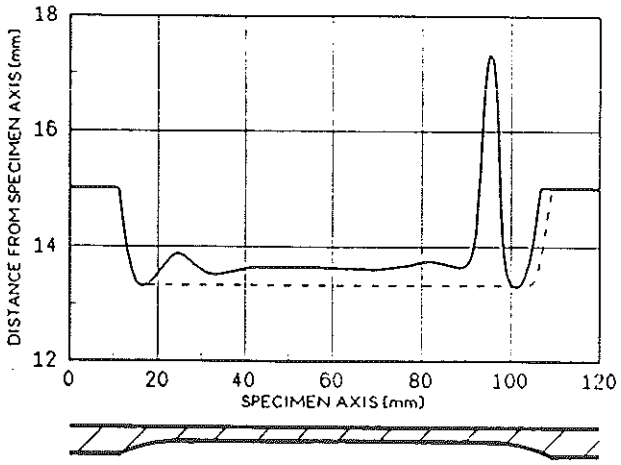

Fig 14 Specimen profile after tension, torsion and internal pressure loading. (The initial specimen profile is indicated by the broken line.)

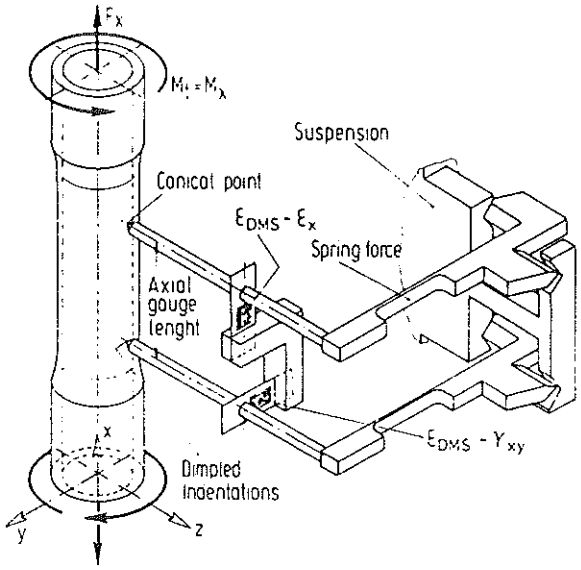

Fig 15 Axial–torsional extensometer (schematic).

7 Design of High-Precision Extensometers

The basic design of an axial–torsional extensometer is illustrated schematically in Fig. 15. Two sensors of bending beam-type equipped with strain gauges are positioned on the specimen. The sensors incorporate ceramic probes which grip the specimen by means of friction. The probes transmit specimen displacements and rotations to the body of the instrument. A requirement in high-precision extensometry is that the strain measurement system should not exhibit any mechancial hysteresis. The design can be said to be effective when axial strain displacement over the range of ± 15 percent does not cause any shear displacement. Careful consideration must also be given to the method of mounting the instrument on the specimen and to its suspension system.

8 Complex Test Procedures

The inelastic deformation behaviour of metallic materials is nonlinear, path dependent, directional with respect to crystalline orientation, irreversible, and generally irrecoverable under any imposed mechanical or thermomechanical load history. Extensive experimentation has been carried out and many proposals of low-cycle and high-cycle fatigue failure criteria have been reported (**6-8, 16**). When the multiaxial strains are out-of-phase, it has been shown that the resulting fatigue life behaviour is often shorter than those for similar in-phase strains in the low-cycle fatigue (**17**). Both, the Tresca and von Mises criteria

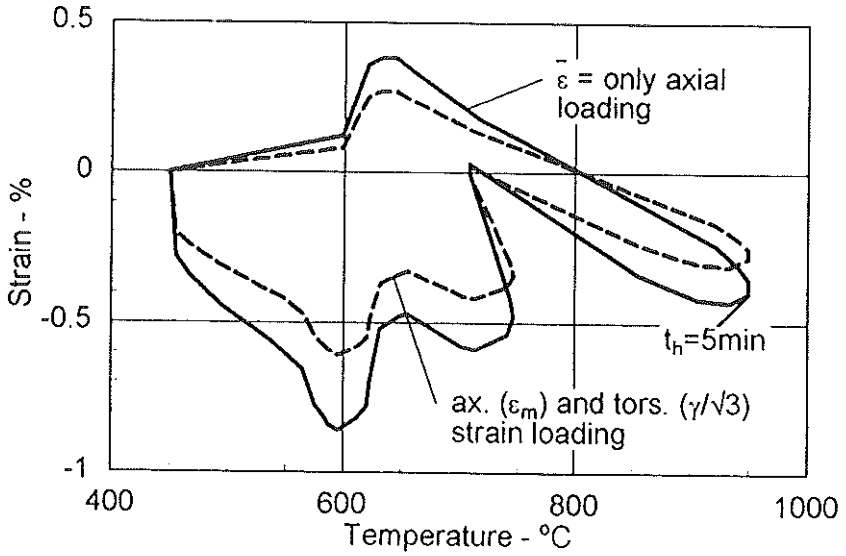

Fig 16 Start up and shut-down axial and shear strain–temperature profile of a blade leading edge.

generally result in over-estimation of (nonconservative) fatigue life for such loading conditions.

The amount of cyclic hardening increases with complexity of the cycle. This is generally attributed to the induced interaction of more slip systems as the principal axes of deformation are rotated. However, not all alloys show this nonproportional cyclic excess hardening effect (**18, 19**). Furthermore, research concerned with thermomechanical loading is increasing, facilitated by recent progress in computer controlled testing machines, and because it is usual for high-temperature components to be subjected to temperature variation as well as mechanical loading. The effect of delays, overshoots and phase differences of thermal, mechanical and net strain components with time, in out-of-phase and in-phase cases in relation to command signal, requires more investigation.

There are two methods of compensating for thermal strain during testing. The thermal strain can be approximated by a function with respect to time, when command signal is then the sum of this thermal strain and the desired mechanical strain. Alternatively both the thermal strain and temperature can be measured and related. Throughout the test, the mechanical strain is then modified in order to compensate for the calculated thermal strain based on the temperature at that moment. Test matrices should be more closely linked to real instances that is to say, to more complex loading cycles. Due to the wide variation in strain–temperature history that a blade experiences a more complex thermomechanical cycle was investigated, Fig. 16, in an attempt to understand the effects of axial and shear strain, temperature and time on fatigue life.

A topic of great interest and importance is the multiaxial ratchetting strain accumulation, taking place under combined steady stress and cyclic stress.

9 Thermocouple Temperature Control

Since the purpose of induction heating is to produce highly localized heating, the correct placement of a thermocouple for temperature control is very important. This should be accomplished without spot welding anything to the actual specimen gauge. Care must be taken to overcome any induction pick-up in the thermocouple or in the control circuitry of the test machine. The thermocouple should be attached perpendicularly to the specimen surface through a gap between the induction coil. It should be noted that in ferromagnetic materials cyclic loading may give rise to corresponding RF (radio frequency) coupling problems, leading in turn to temperature variations.

10 Data Acquisition

The most commonly used parameters in fatigue criteria are

(1) shear strain and normal strain;
(2) shear strain and normal stress;
(3) shear stress and normal stress;
(4) energy;
(5) bending and torsional stresses.

This data will be required, for example, for the assessment of fatigue theories. Computerized data acquisition is not subject to the inaccuracies accumulated through the slow response of a mechanical device. However, the sample rate must be adjusted to obtain a continuous date printout with acceptable gaps. The position of the points in relation to the data curve are very important, especially in the case of stress–strain loops.

The digitilized test data can be quickly processed and a wide variety of information readily extracted using suitable software.

11 Concluding Remarks and Future Directions

Standards-orientated research into the response of a material to multiaxial loading conditions should be encouraged. In particular, information is needed about the effects of specimen shape including surface finish and axiality of loading, and most importantly, information is needed in order to define failure and time-dependent behaviour. Such standards would enable investigators to decide on the most appropriate technique to study the wide range of service conditions.

An important direction for multiaxial fatigue is the development of measurement techniques up to the micron range. Fundamental understanding of fatigue

and fracture requires measurements of deformation within individual grains and across grain boundaries.

Measurement techniques for difficult environments is another important direction for future investigations. High temperature and high rates of deformation present experimental difficulties that are not encountered in conventional laboratory experiments.

References

(1) EVANS, W. K. (1972) Deformation and failure under multiaxial stress – a survey of laboratory techniques and experimental data, *Note No. NT 833*, National Gas Turbine Establishment, Hants. UK.

(2) ANDREWS, J. M. H. and ELLISON, E. G. (1973) A testing rig for cycling at high biaxial strains, *J. Strain Analysis*, **8**, (3), pp. 168–175.

(3) BROWN, M. W. (1982) Low cycle fatigue testing under multiaxial stresses at elevated temperature, in *Measurement of High Temperature Mechanical Properties of Materials*, (ed. by M. S. Loveday, M. F. Day, B. F. Dyson), London, Her Majesty's Stationary Office, pp. 185–203.

(4) BROWN, M. W. (1983) Multiaxial fatigue testing and analysis, in *Fatigue Testing and Analysis in Fatigue at High Temperature*, (ed. by R. P. Skelton), Applied Science Publishers, London, pp. 97–133.

(5) FOUND, M. S., FERNANDO U. S. and MILLER, K. J. (1985) Requirements of a new multiaxial fatigue testing facility, in *ASTM STP 853*, (K. J. Miller and M. W. Brown, Eds.), ASTM, Philadelphia, pp. 11–23.

(6) GARUD, Y. S. (1981) A new approach to the evaluation of fatigue under multiaxial loadings, *J. Test Eval.*, **9**, pp. 165–178.

(7) BROWN, M. W. and MILLER, K. J. (1982) Two decades of progress in the assessment of multiaxial low-cycle fatigue life, in *Low-Cycle and Life Protection, ASTM STP 770*, ASTM, pp, 482–499.

(8) ELLYIN, F. and VALAIRE, B. (1985) Development of fatigue failure theories for multiaxial high strain conditions, *SM Archives*, **10**, pp. 45–85.

(9) RAHKA K. and LAIRD, C. (1986) Poisson's ratio as determined for elastic and plastic deformation and for monotonic and cyclic loading, Part I: Critical review, *J. Test. Eval.*, **14**, pp. 173–180.

(10) ELLYIN, F., GOLOS, K. and XIA, Z. (1991) In-phase and out-of-phase multiaxial fatigue, *J. Eng. Mat. Tech.*, **113**, pp. 112–118.

(11) PARSONS, M. W. and PASCOE, J. K. (1973) Development of a biaxial fatigue testing rig, *J. Strain Anal.*, **10**, pp. 1–9.

(12) WILSON, I. H. and WHITE, D. J. (1971) Cruciform specimens for biaxial fatigue tests: an investigation using finite-element analysis and photoelastic coating techniques, *J. Strain Analysis*, **6**, pp. 27–37.

(13) TIPTON, M. S. and NELSON, D. (1985) Fatigue life predictions for a notched shaft in combined bending and torsion, *ASTM STP 853*, (K. J. Miller and M. B. Brown, Eds.), ASTM, Philadelphia, pp. 518–550.

(14) SHEWCHUK, J., ZAMRIK, S. Y. and MARIN, J. (1968) Low cycle fatigue of 7075–T61 aluminium alloy in biaxial bending, *Exp. Mechanics*, **8**, pp. 506–512.

(15) AELKIN, P. and HARVEY, S. J. (1989) *Effects of Biaxiality in Biaxial and Multiaxial Fatigue*, EGF3, (Ed. by M. W. Brown and K. J. Miller), Mechanical Engineering Publications, London, pp. 173–184.

(16) KANAZAWA, K., MILLER, K. J. and BROWN, M. W. (1977) Low cycle fatigue under out-of-phase loading conditions, *J. Eng. Mat. Techn.*, **99**, pp. 222–228.

(17) CHAN, K. S., LINDHOLM, U. S., BODNER, S. R. and NAGY, A. (1990) High temperature inelastic deformation of B1900 + Hf alloy under multiaxial loading: theory and experiment, *J. Eng. Mat. Techn.*, **112**, pp. 7–14.

(18) ZIEBS, J., MEERSMANN, J. and KUHN, H.-J. (1994) Effects of proportional and nonproportional straining sequences on hardening/softening behaviour of IN 738 LC at elevated temperatures, *Eur. J. Mech. A/Solids*, **13**, pp. 605–619.
(19) ZAMRIK, S. Y., GOTO, T. (1968) The use of octahedral shear strain in biaxial low cycle fatigue T., *Materials Technology of Interamerican Approach*, ASME, N.Y., pp. 551–562.